Journal of Solid State Chemistry 184 (2011) 2023–2032

Contents lists available at ScienceDirect

Journal of Solid State Chemistry

journal homepage: www.elsevier.com/locate/jssc

A very promising piezoelectric property of Ta_2O_5 thin films. I: Monoclinic–trigonal phase transition

M. Audier [a,*], B. Chenevier [a], H. Roussel [a], L. Vincent [b], A. Peña [c], A. Lintanf Salaün [d]

[a] Laboratoire des Matériaux et du Génie Physique, UMR CNRS 5628, Minatec - INP Grenoble, 3 parvis Louis Néel, BP 257, 38016 Grenoble Cedex 1, France
[b] CIME Nanotech Minatec, Microsystèmes et capteurs, F-38016 Grenoble Cedex 1, France
[c] Institut Néel - CNRS/UJF, Dpt. Matière Condensée, Matériaux et Fonctions, F-38042 Grenoble, France
[d] L2MA, CEA LETI D2NT, F-38054 Grenoble, France

ARTICLE INFO

Article history:
Received 6 April 2011
Received in revised form
28 May 2011
Accepted 1 June 2011
Available online 12 June 2011

Keywords:
Tantalum oxide
Ceramic thin film
Phase transition
Transmission electron microscopy
X-ray diffraction
X-ray photoelectron spectroscopy

ABSTRACT

Ceramic thin films of tantalum oxide of a new trigonal structure ($a=12.713(7)$ Å, $\alpha=28.201(0)^\circ$, space-group $R3$) were produced by thermal treatments of amorphous deposits on (001)Si wafers, either by electrostatic spray deposition or by injection metal-organic chemical vapor decomposition. This trigonal phase comes from the transformation of a monoclinic phase 11L- or 25L-Ta_2O_5. The transformation is reversible under oxygen atmosphere and, from results of TEM investigations, occurs mainly via atomic motions along the z unique axis of the monoclinic structure parallel to the polar three-fold axis of the trigonal structure. The non-centrosymmetry and direction of polar axis of the trigonal phase, identified by high resolution TEM imaging, indicate a possibility of very high electric dipole moments linked to a strong piezoelectricity. From results of XPS analyses of both monoclinic and trigonal structures, the binding energies remain similar to those of Ta_2O_5. As the formation of the trigonal structure gives rise to an important volume expansion, stresses induced in ceramic thin films are likely influencing both properties of birefringence and piezoelectricity which are presented in a separated article (part II). It is mentioned that the formation of trigonal phase does not occur in bulk Ta_2O_5 samples, for which an incommensurate phase transition has been observed in a previous work.

1. Introduction

The tantalum pentoxide Ta_2O_5 and related compounds in the system $Ta_2O_5-WO_3$ are known to exhibit various commensurate [1–8] and incommensurate [9–12] structures at low temperature, i.e. for $T\lessapprox 1320$ °C where Ta_2O_5 undergoes a structural transformation [13]. In a quite recent article, Grey et al. [8] have yielded a detailed review of the crystal chemistry of these phases and determined a new structure called 19L-Ta_2O_5 by single crystal X-ray diffraction. In the notation of structure, L stands for low temperature phase and 19 is a multiple integer (m) of a parameter b_o of an orthorhombic sub-cell proposed by Lehovec [14] ($a_o=6.20$ Å, $b_o=3.66$ Å, $c_o=3.89$ Å). The approach of Lehovec has been proved to be very useful since different L-Ta_2O_5 related commensurate structures with different multiplicities of 5, 8, 11, 13, 14 and 19 were identified ([8] and references there-in). As the m values obey to specific rules [3,8], a general model proposed by Grey et al. explains not only the structural chemistry in the known mL-Ta_2O_5-related structures but also allows one to predict other structures. This was the case for a new 25L-Ta_2O_5 structure that we have observed in a bulk material [15]. In the model of Grey et al., all the structures are monoclinic, based on packing of similar polyhedra corresponding to TaO_6 octahedra and TaO_7 pentagonal bipyramids which, assembled in different sequences, exhibit a symmetry either P or C. Besides, the space-group of the 19L-Ta_2O_5 structure being centrosymmetric ($C112/m$), application of this model implies that all m L-Ta_2O_5-related structures are centrosymmetric.

Piezoelectric properties have been found by a number of authors [16–22] in crystallized Ta_2O_5 thin films obtained by sputtering techniques. As structures must be non-centrosymmetric, Ta_2O_5 crystal structures in thin films could be different of those observed in bulk materials. Nakagawa et al. [16–19] report that Ta_2O_5 thin films with an oriented monoclinic structure (the β phase [1]) belonging to point group m ($a_\beta=7.31$ Å, $b_\beta=15.53$ Å, $c_\beta=21.54$ Å, $\beta=120.35^\circ$) exhibit a piezoelectric property comparable to ZnO and can be used as surface acoustic-wave device with good characteristics at high temperature. The monoclinic β phase is actually related to the Lehovec sub-cell as $\mathbf{a}_\beta=2\mathbf{b}_o$, $\mathbf{b}_\beta=4\mathbf{c}_o$, $\mathbf{c}_\beta=3\mathbf{a}_o-3\mathbf{b}_o$ [1]. Qualitative results on the surface acoustic-wave properties of Ta_2O_5 films were also published by Viljoen and Jooste [20,21]. Parmentier et al. [22] report a piezoelectric property of Ta_2O_5 thin films of 11L-Ta_2O_5 structure of space-group $Pmm2$ according to the International Centre for

* Corresponding author. Fax: +33 456529301.
E-mail address: Marc.Audier@grenoble-inp.fr (M. Audier).

0022-4596/$ - see front matter © 2011 Elsevier Inc. All rights reserved.
doi:10.1016/j.jssc.2011.06.001

Table 1
Structures of Ta_2O_5 thin films prepared by ESD and i-MOCVD as a function of different thermal treatments.

Sample type (thickness)	Thermal treatments (tt)	Cooling rate	Structures
ESD 20 nm	tt1: 980 °C, 1 h, O_2	5 °C min^{-1}	Monoclinic 11L-Ta_2O_5 + trigonal (R3)
	(tt1)+tt2: 980 °C, 1 h, O_2	Quenched	Monoclinic 11L-Ta_2O_5 only
	(tt1+tt2)+tt3: 980 °C, 1 h, O_2	5 °C min^{-1}	Monoclinic 11L-Ta_2O_5 + trigonal (R3)
i-MOCVD 67 nm	850 °C, 1 h, O_2	quenched	Monoclinic 25L-Ta_2O_5
i-MOCVD 67 nm	850 °C, 2 h, O_2	5 °C min^{-1}	Monoclinic 25L-Ta_2O_5
i-MOCVD 67 nm	tt1: 850 °C, 1 h, N_2	5 °C min^{-1}	Monoclinic 25L-Ta_2O_5
	(tt1)+tt2: 850 °C, 2 h, N_2	5 °C min^{-1}	Monoclinic+ trigonal (R3)

Diffraction Data [23].[1] Using an extrinsic Fabry–Perot interferometer, the relative thickness variation under an oscillating electrical field measured by these authors was ≈13 pm/V while they were expecting a value of 200 pm/V. However, we did not find any reference for such a value.

In the present work, we have studied the structure of crystallized Ta_2O_5 thin films, obtained initially in an amorphous state by two different techniques—electrostatic spray deposition (ESD) and injection metal-organic chemical vapor decomposition (i-MOCVD). These films were crystallized through different thermal treatments (Section 2). The general model for L-Ta_2O_5 structures proposed by Grey et al. [8] was used to identify different monoclinic structures observed by high resolution transmission electron microscopy (HRTEM) (Section 3.1). Characteristics of a reversible phase transformation between these monoclinic structures and a trigonal structure are presented in Section 3.2. From the symmetries observed by HRTEM imaging, the trigonal structure is identified to be non-centrosymmetric (Section 3.3). The mechanism of the transformation is analyzed and with respect to both solutions of space-groups $R3c$ and $R\bar{3}c$ deduced from the reflection conditions of a $\theta/2\theta$ X-ray diffraction pattern, it is shown that the actual space-group is $R3$ but with reflection conditions resulting of particular symmetries between atomic sites. As an oxygen diffusion due to a partial reduction of Ta_{5+} cations could be considered, XPS analyses performed on both structures, indicate that the stoichiometry remains actually similar to this of Ta_2O_5. On account of the present results, we conclude that an interesting property of piezoelectricity could be expected for the trigonal Ta_2O_5 phase. For this reason, preliminary results on a study related to properties of birefringence and piezoelectricity of these structures will be presented in a following paper (part II).

2. Experimental

Fabrications of Ta_2O_5 thin films have been reported in articles from Lintanf Salaün et al. [24,25] for the ESD and e.g. Fang et al. [26] for the i-MOCVD. The chemical precursors were the tantalum (V) tetraethoxide pentanedionate ($Ta(OC_2H_5)_4(CH_3\ COCHCOCH_3$, Alfa Aesar, 99.99% Ta) for ESD and the tantalum tetraethoxide dimethylaminoethoxide ($Ta(OC_2H_5)_4O(CH_2)_2N(CH_3)_2$, Multivalent Laboratory, Ltd., UK[2]) for i-MOCVD. Both types of film were deposited on (001)Si wafers in an amorphous state. Their thickness were in a range of 20–40 nm for the ESD and 5–100 nm for the i-MOCVD. In the present study a series of thermal treatments were applied in order to study their crystallization by TEM and $\theta/2\theta$ X-ray diffraction. The experimental conditions used for these thermal treatments are reported in Table 1 with the film thickness and results on the observed structures. Through three successive thermal treatments (noted tt1, tt2 and tt3 in Table 1) performed on a film prepared by ESD at 980 °C under oxygen, it was shown that a 11L-Ta_2O_5 monoclinic phase transforms into a trigonal phase by slow cooling and that this transformation is reversible with temperature. The formation of the trigonal phase also occurs in a film prepared by i-MOCVD through a slow cooling from 850 °C under nitrogen atmosphere but not under oxygen. In this case, one might assume that thermodynamic equilibria with different Ta_2O_5 (or Ta_xO_y) structures depend on the oxygen pressure. For instance, an increase of the oxygen pressure at 850 °C could stabilize the monoclinic phase.

TEM observations were carried out on a JEOL 2011 UHR (i.e. for ultra high resolution) and X-ray diffraction diagrams on tantalum oxide films were recorded from a $\theta/2\theta$ goniometer using the Cu$K\alpha 1$ wavelength. TEM samples were small fragments, obtained by scratching the film surface with a diamond tip, which were deposited on copper grids coated with holey carbon films.

3. Results

3.1. Structure of the crystallized films after quenching

Fig. 1(a,b) shows TEM bright field images of the crystallized films prepared by ESD and i-MOCVD after a rapid cooling from 980 and 850 °C, respectively. Corresponding selected area electron diffraction (SAED) patterns of [001] zone axis and images of the film cross-sections are shown in insets. Both these parts of films are constituted of domains of monoclinic phase of 3 (or 6) different orientations related by angles of 120° (or 60°) around the [001] axis. Structural defects in between domains of the film prepared by ESD (see arrows in Fig. 1(a)) appear to be aligned along directions related by rotation angles of 120°. These microstructures gives rise to a pseudohexagonal symmetry observed on SAED patterns but from which Bravais lattices cannot actually be identified. The observed reflections were nevertheless found to be in agreement with $hk0$ reflections of the Lehovec sub-cell. Only the large contrast periodicities of about 4.5 ± 0.6 nm observed on these images indicate large cell parameters of the type $b = mb_o$. These films did not seem to be textured because different crystallographic orientations normal to the (001)Si substrate surface have been observed.

[001] sections of Bravais lattices could be identified from HRTEM images associated to their fast Fourier transform (FFT). A projection of the atomic structure normal to the [001] direction was then derived from the structural rules of Grey et al. [8] in order to check structural agreements between HRTEM observations and image simulations calculated by the multislice method [27]. For instance, Fig. 2(a) shows a HRTEM image of a very thin fragment of the film prepared by ESD. The focalization of the

[1] Such a space-group $Pmm2$ is not mentioned in Ref. [7] cited on the JCPDS card No. 25-0922. Actually, only x, y atomic coordinates have been refined in the plane group pm with z coordinates assumed to be either 0 or $\frac{1}{2}$.

[2] Formerly Inorgtech, Ltd., UK, then Epichem, Ltd., UK and after Multivalent Laboratory, Ltd., UK.

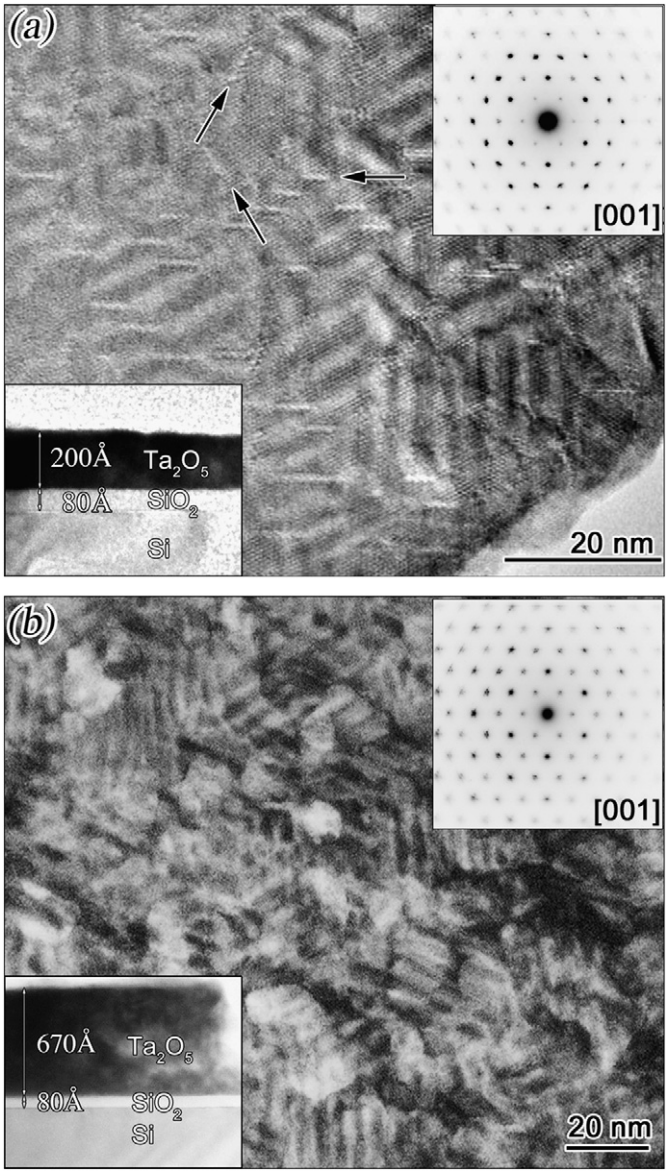

Fig. 1. Bright field TEM images of the crystallized films of different monoclinic structure prepared by ESD (a) and i-MOCVD (b) within insets their corresponding SAED patterns of [001] zone axis and images of sample cross-sections. The arrows in (a) point to structural defects between domains.

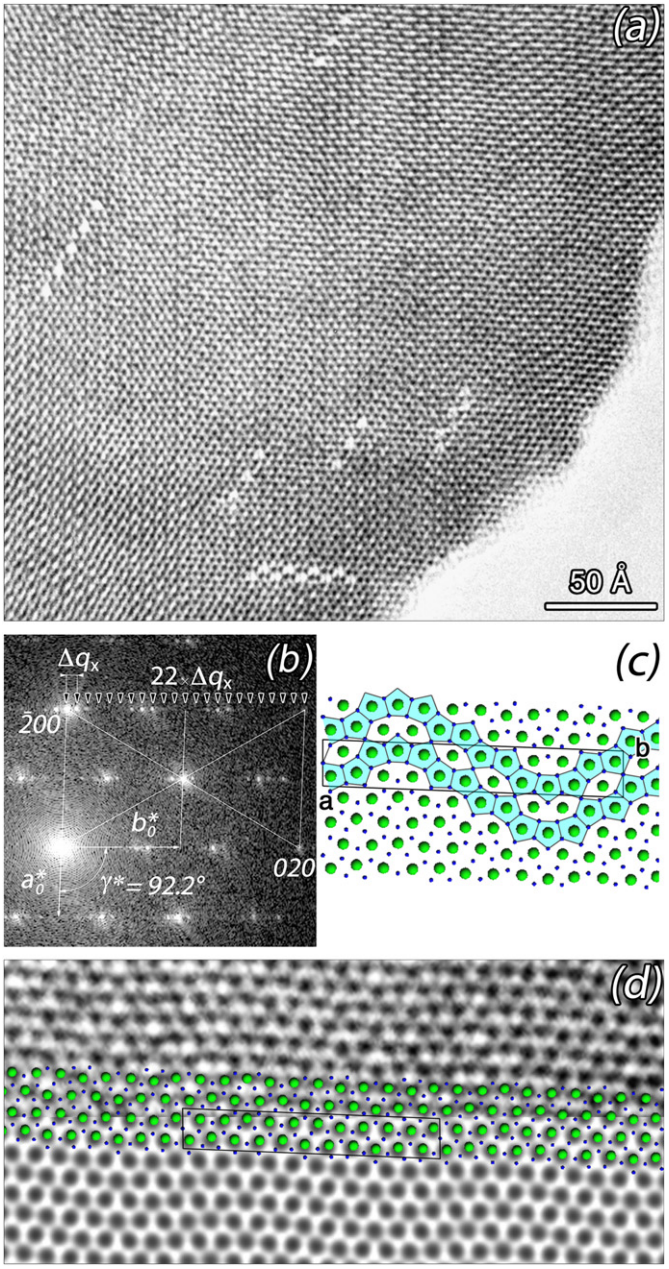

Fig. 2. (a) HRTEM image of a Ta_2O_5 film obtained by ESD and rapidly cooled down from 980 °C; (b) FFT corresponding to selected circular area situated in between the observed structural faults; (c) structural model for 11L-Ta_2O_5 derived from crystallographic data and structural rules of Grey et al. [8] and (d) comparison between an enlarged image of (a) and a simulated image. (For interpretation of the references to color in this figure legend, the reader is referred to the web version of this article.)

objective lens was close to the condition of Scherzer defocus $\Delta f = -1.2(C_s\lambda)^{1/2} = -42.5$ nm for a spherical aberration coefficient $C_s = 0.5 \times 10^6$ nm and an electron wavelength $\lambda = 2511 \times 10^{-6}$ nm. The orientation of the crystal fragment is of [001] zone axis from the FFT of the image in (b). This FFT is related to a selected circular area situated in the middle part of the image in between the structural defects. Both spots, indexed as 200 and 020 correspond to reflections of the Lehovec sub-cell. Thus, assuming that the *hk*0 rows of spots parallel to the 0*k*0 row are periodic with a period Δq_x, one obtains in the direct space a period $b = 22d_{020} = 22b_o/2 = 40.26$ Å and $m = 11$. The structure of 11L-Ta_2O_5 can be assumed here to be monoclinic of space-group $P112/m$ or $P112$ due to a γ^* angle between $\mathbf{a}_o^*$ and $\mathbf{b}_o^*$ of 92.2° and no condition on *hkl* reflections. The [001] projection of 11L-Ta_2O_5 as deduced from the structural rules of Grey et al. [8,15] is represented in Fig. 2(c). Ta atoms at $z=0$ are represented by large balls of green color and O atoms at $z=0$ by small blue balls. There is another layer of oxygen atoms at $z = \frac{1}{2}$ (not represented) which *x*, *y* coordinates correspond to those of Ta atoms at $z=0$. As described by Grey et al. Ta atoms occupied either the center of distorted TaO_7 pentagonal bipyramids (i.e. the pentagon in blue on the [001] projection) or the center of distorted TaO_6 oxygen octahedra which are in between parallel folded chains of edge-shared TaO_7 polyhedra. Let us note that from X-ray structural refinements, Grey et al. [8] have also found that Ta_2O_5 stoichiometry is achieved through Ta interstitial atoms situated at $z = \frac{1}{2}$ next to TaO_6 octahedra (as previously suggested by [14]). But, other authors [9–12] have considered oxygen vacancies instead of Ta interstitial atoms.[3] Also let us point out that if the *b* cell parameter of 11L-Ta_2O_5 correspond

[3] As there are 22 Ta and 58 O in the unit cell, one can consider either 3 O vacancies or 0.6 Ta interstitial atoms in order to achieve a Ta_2O_5 stoichiometry.

to 11 b_o, the distance $b_o/2$ corresponds only to an average distance between the successive planes of Ta atoms parallel to (010). Along the [010] direction, Ta atoms form two types of zig-zag rows which are best seen at a glancing angle. The comparison between an enlarged central part of the image (a) and the [001] projection of the 11L-Ta_2O_5 structure superimposed to a simulated HRTEM image is shown in Fig. 2(d). This simulated image was obtained for a sample thickness of 2.7 nm and a defocus value of −39 nm, which is close to the Scherzer defocus (−42.5 nm). Similar simulated images were also obtained for thickness variations of 1–2.9 nm and defocus values of −20 to −40 nm. The [001] Ta–O atomic columns correspond to black dots while O columns are not visible. The zig-zag rows of Ta–O columns appear to be similar between both simulated and HRTEM images, which confirms a 11L-Ta_2O_5 structure and the validity of structural rules proposed by Grey et al. [8]. In this case, however, study of the piezoelectric behavior of this 11L-Ta_2O_5 structure as it has been done by Parmentier et al. [22] requires to consider a few atomic shifts along the z axis in accordance with the symmetry operator of the non-centrosymmetric space-group $P112$ (i.e. /x, y, z/ $\bar{x}$,$\bar{y}$,z/ which through a shear parallel to [100] (or [010]) (such that $\gamma = 90^\circ$) could actually be related to the symmetry operators of orthorhombic space-group $Pmm2$ (/x, y, z/$\bar{x}$,$\bar{y}$,z/ x,$\bar{y}$,z/ $\bar{x}$,y,z/ with no condition on hkl reflections [23]).

The structural defects within the Ta_2O_5 thin film prepared by ESD can be analyzed using a superimposed [001] projection of the 11L-Ta_2O_5 structure. From the representation shown in Fig. 3 and in Fig. 1(a) they appear to correspond to missing 001 columns of Ta atoms along {1110} and {100} planes of the 11L-Ta_2O_5 structure. Such a feature could seem surprising since either Ta interstitial atoms or oxygen vacancies are expected in this structure. However, we cannot identify if oxygen vacancies (or cationic impurities) are associated with these Ta vacancies for satisfying a charge equilibrium.

A similar type of study has been performed on the Ta_2O_5 film prepared by i-MOCVD and rapidly cooled down. The 25L-Ta_2O_5 monoclinic structure ($a = 6.20$ Å, $b = 25b_o = 91.5$ Å, $c = 3.89$ Å, $\gamma \approx 90^\circ$, $C112/m$ (or $C112$)) was identified as it has previously been found in a bulk material [15].

3.2. Phase transformation

The monoclinic-to-trigonal transformation occurs by slow cooling at 5 °C min^{-1}, from 980 °C under O_2 for the ESD film and from 850 °C under N_2 for the i-MOCVD film (Table 1). Lamellae of trigonal phase formed within the monoclinic phase can be observed in the central part of the bright field image in Fig. 4(a). The HRTEM image (b) shows that interfaces between both phases are planes and that the trigonal structure exhibits, a priori, a twinning. On account of the electron diffraction patterns, related to selected area of interfaces between both phases (Fig. 4(c)), the habit planes between both trigonal and monoclinic structures are {111} parallel to {001}, respectively and the twinning would be of (111) type. Reflections corresponding to the Lehovec sub-cell of the monoclinic structure are indexed on the left part of each pattern and those corresponding to the trigonal structure (rhombohedral cell) are indexed in the right part. The indexing of the trigonal structure is such that $l = 2n$ for

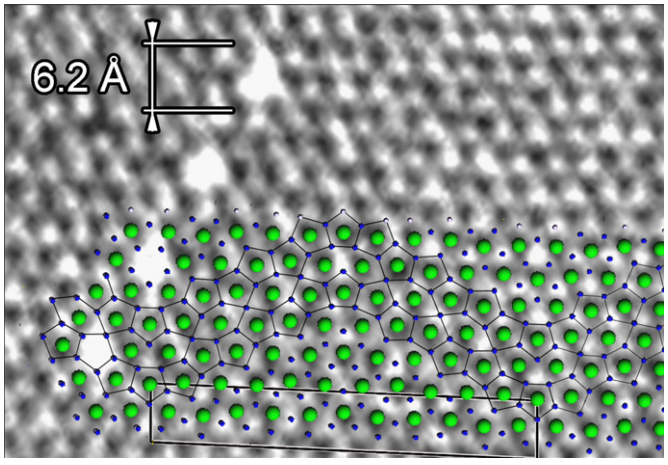

Fig. 3. Structural defects corresponding to alignments of columns of Ta and probably O vacancies.

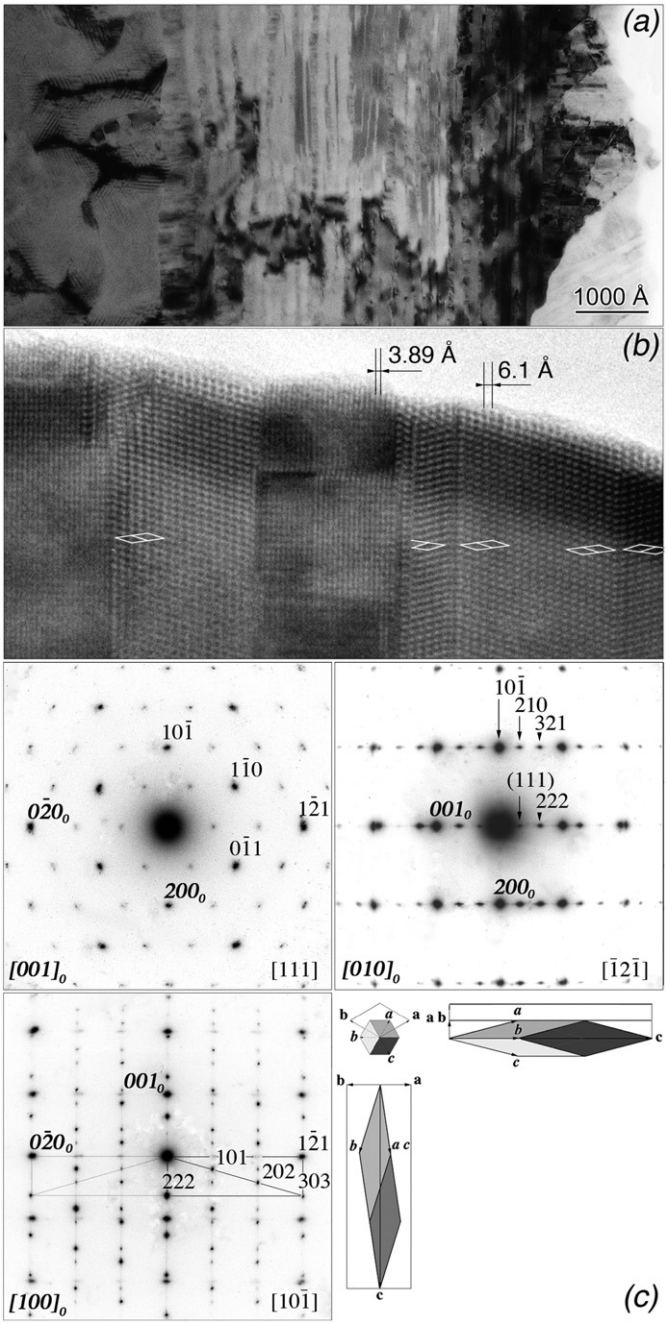

Fig. 4. (a) TEM bright field image of the Ta_2O_5 film prepared by i-MOCVD, cooled down at 5 °C min^{-1} after a thermal treatment at 850 °C under N_2 for 1 h; (b) HRTEM images related to the interface between both monoclinic and trigonal phases; (c) set of corresponding SAED patterns from which a trigonal structure can be identified. Crystallographic orientational relationships with the monoclinic phase were deduced from these patterns.

hhl reflections. The *hhh* reflections with *h* odd observed on the pattern of $[\bar{1}2\bar{1}]$ zone axis but not on the pattern of $[10\bar{1}]$ zone axis result of double diffraction effects. Therefore, on account of reflection conditions, the space-group of the trigonal structure could be either $R3c$ or $R\bar{3}c$. The occurrence of (111) twinned lamellae can be interpreted from the two possibilities for orienting the trigonal phase with respect to the pseudo six-fold symmetry of the monoclinic phase.

The crystallographic orientational relationships (COR) deduced from diffraction patterns are: $[111]_R \| [001]_o$, $[\bar{1}2\bar{1}]_R \| [010]_o$ and $[10\bar{1}]_R \| [100]_o$, where subscripts *R* and *o* stand for the rhombohedral cell and the orthorhombic sub-cell of Lehovec, respectively.

By reference to the cell parameter values of the orthorhombic sub-cell, those of the trigonal structure were determined as corresponding to $a \approx 12.7$ Å, $\alpha \approx 28.2°$.

Note that TEM observations of sample cross-sections after phase transformation in nitrogen atmosphere showed that the thickness of Ta_2O_5 and SiO_2 films remained nearly unchanged.

Similar results were obtained for Ta_2O_5 films prepared by ESD. An increase of the SiO_2 film thickness was however observed because thermal treatments were performed in oxygen atmosphere (Table 1).

Cell parameter values were then accurately determined by $\theta/2\theta$ X-ray diffraction using the fine double diffraction reflection 002 of the Si substrate as reference, i.e. $d_{002} = 2.7155$ Å (Fig. 5). From a refinement of cell parameter values, we have obtained $a = 12.713(7)$ Å, $\alpha = 28.201(0)°$ for rhombohedral axes and $a_{hex} = 6.194(6)$ Å, $c_{hex} = 36.599(9)$ Å, $\gamma = 120°$ for hexagonal axes. The a_{hex} value appears almost equal to this of a_o (6.20 Å). Both lattices of monoclinic and trigonal structures are incommensurate along their habit planes $(111)_R \| (001)_o$ and along their axes $[111]_R \| [001]_o$ (i.e. $c_{hex}/c_o = 9.4087$). From the X-ray diffraction pattern observed in Fig. 5, the majority phase corresponds to the trigonal structure. The most intense reflections of both trigonal and monoclinic phases are 222 and 001_o, respectively. The possibility of a fiber texture of axis $[111]_R \| [001]_o$ normal to the substrate surface, which would be different of the strong texture of $(110)_o$ (or $(200)_\beta$) planes parallel to the substrate surface observed by Nakagawa et al. [17] has been envisaged. However, the result of an analysis of a {123} pole figure by X-ray diffraction on a texture goniometer showed no ring 123 at a polar angle of 63.081° corresponding to the angle between the $[111]_R$ axis normal to the sample surface and the diffracting vectors of 123 reflections.

One can note that a reflection 333 of very small intensity, indicated in brackets in Fig. 5, is not allowed by the reflection conditions of space-groups $R3c$ and $R\bar{3}c$. Although such a reflection is not observed on SAED patterns, other possibilities of space-groups corresponding to maximal non-isomorphic subgroups cannot be excluded, i.e. the $R3$ subgroup of $R3c$ and both $R32$ and $R\bar{3}$ subgroups of $R\bar{3}c$. Such subgroups will be considered in the next section for interpreting HRTEM images.

A reversibility of this phase transformation has been found through different thermal treatments applied to the Ta_2O_5 film prepared by ESD (Table 1). Compared to the monoclinic phase, the trigonal structure can be considered as the stable state at low temperature since it is only formed by slow cooling. A particularity of this transformation would be therefore occur with a symmetry increase on cooling (if it occurs without oxygen diffusion). Such an unusual behavior has also been found for transitions in ferroelectric phases of potassium sodium tartrate $KNaC_4)H_4O_6–4H_2O$ (or Rochelle salt) and $Ba_2NaNb_5O_{15}$ [28].

TEM observations of the growth front of lamellae of trigonal structure within the monoclinic phase show that the transformation occurs with a rational ratio of 3 periods of 001_o fringes for 2 periods of 222_R fringes (Fig. 6). On the image (a) viewed along a zone axis $[010]_o \| [\bar{1}2\bar{1}]_R$, the growth front of a lamellae of thickness $2 \times d_{(222)R}$ comes from the transformation of monoclinic phase of thickness $3 \times d_{(001)o}$. If 010 rows of black spots observed in this image correspond to (001) planes of Ta–O atoms of the monoclinic structure, then we can assume that two adjacent planes come together with a rearrangement in three-fold symmetry to form a layer of Ta–O atoms in the trigonal structure. For a thicker lamellae of $4 \times d_{(222)R}$ observed in (b) along a zone axis $[100]_o \| [10\bar{1}]_R$, this gathering of two adjacent planes (001) Ta–O into one single layer is periodic with a period of $3 \times d_{001}$ (see periodic arrows at $3 \times d_{001}$ corresponding to arrows at $2 \times d_{222}$). The third image (c) shows that the ratio of periods is still 3/2 (15 periods of 001_o fringes for 10 periods of 222_R fringes). Measuring each lamellae thickness on this image (i.e. corresponding to

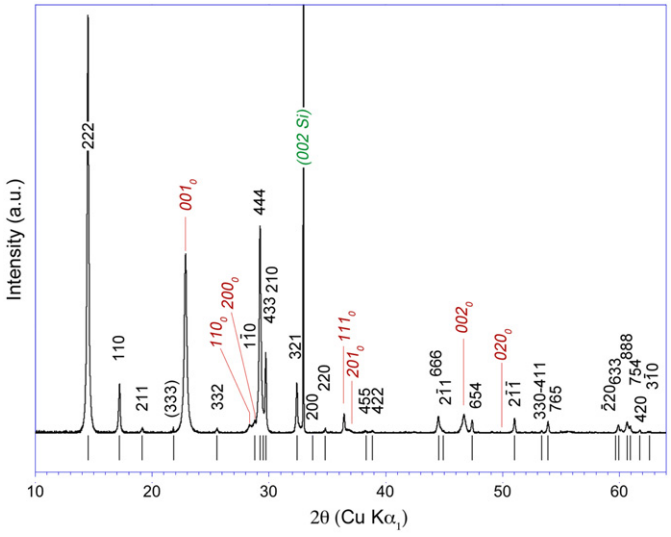

Fig. 5. $\theta/2\theta$ X-ray pattern of the tantalum oxide film prepared by i-MOCVD, cooled down at 5 °C min^{-1} after a thermal treatment at 850 °C under N_2 for 1 h. Indexing of the reflections are in black for the trigonal phase, green for the Si substrate and red for the orthorhombic sub-cell of Lehovec. (For interpretation of the references to color in this figure legend, the reader is referred to the web version of this article.)

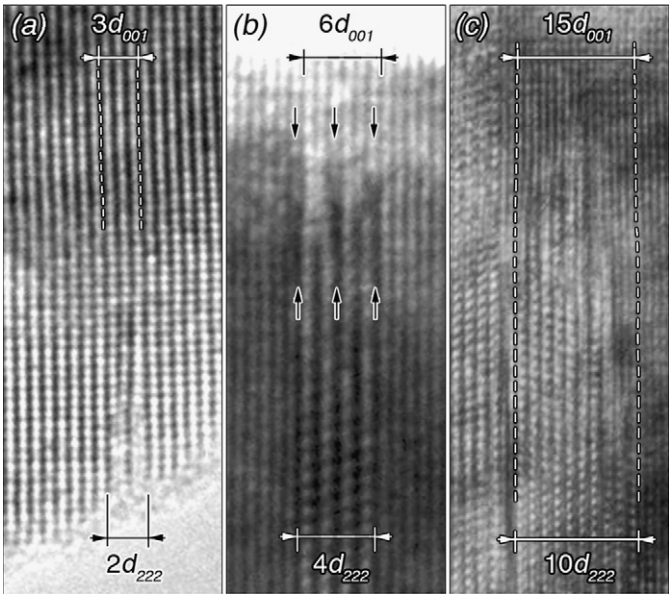

Fig. 6. Growth fronts of lamellae of different thicknesses where it appears that the ratio of periods for the transformation between the monoclinic and trigonal phases is 3/2.

15 $\times d_{001}$ and 10 $\times d_{222}$), one checks that the ratio of length is in agreement with the expansion ratio deduced from the cell parameter values, i.e. $((2\times\frac{1}{6}c_{hex})/3\times c_o)=1.045$.

A rational ratio of periods between both monoclinic and trigonal structures is in agreement with a property of reversibility for the transformation. The phase transformation is apparently displacive although it is associated to an important expansion ratio along the ternary axis (i.e. 1.045). The overall volume expansion ratio can be estimated with respect to the volume of the Lehovec sub-cell ($V_o=a_ob_oc_o$); one has:

$$\frac{a_{hex}^2}{a_ob_o\sqrt{3}}\times\frac{c_{hex}}{9c_o}=\frac{3}{2}\frac{V_{hex}}{V_o}=\frac{9}{2}\frac{V_R}{V_o}0=\frac{9}{2}a_R^3\frac{\sqrt{1-3\cos^2\alpha+2\cos^3\alpha}}{a_ob_oc_o}=1.0207$$

Conjointly to the expansion ratio along the $[111]_R\|[001]_o$ axes, there is a slight radial contraction of (001) monoclinic planes of pseudohexagonal symmetry into (222) rhombohedral planes of $(a_h^2/a_ob_o\sqrt{3})^{1/2}=0.988$.

Assuming that the Lehovec sub-cell contains 1 Ta_2O_5 formula unit in average, the rhombohedral cell (V_R) might contain 4.5 Ta_2O_5 formula units, i.e. 9 Ta atoms and 22.5 oxygen atoms, which would imply oxygen vacancies if tantalum cations are all Ta^{5+}. But a phase transformation occurring via oxygen diffusion and a partial reduction of Ta^{5+} into Ta^{4+} might also be considered. In this case the number of oxygen could be reduced to an integer.

Let us note that, in the case of a non-centrosymmetric structure, dipole moments can be formed in each crystal grain due to stresses generated by the volume expansion. But, the resulting polarization, corresponding to the vector sum of dipole moments, must be null since the vector sum of stresses is also null in isotropic polycrystalline films.

3.3. Space-group analysis

In this section a space-group analysis of the trigonal phase is reported and a possible model of atom rearrangement at the monoclinic-to-trigonal transformation is proposed.

From the International tables for crystallography [29], the symmetry of special projections along [111], $[1\bar{1}0]$ and $[2\bar{1}\bar{1}]$ of trigonal structures of space-group $R3c$, $R\bar{3}c$ and related subgroups are different (Table 2).

In most cases the non-centrosymmetry of piezoelectric phases, for instance, related to a perovskite-type structure cannot be identified by HRTEM imaging because the off-center shifts of cations are very small. As a consequence the observed symmetry of special projections correspond to those of centrosymmetric space-groups. In the present case, however, the departure to centrosymmetry appears to be very pronounced as it is unambiguously identified from high resolution images of $[\bar{1}2\bar{1}]$ zone axis (Fig. 7). Along this zone axis the pattern of large white dots exhibits a symmetry $p1g1$ corresponding to two horizontal glide planes, i.e. reflections through mirror planes followed by displacements by half unit cell parallel to glide planes (see the rectangular unit cell represented in Fig. 7(b) with glide planes represented by dotted lines). From the projection of the rhombohedral unit cell, with an origin at the intersection of a glide plane with a vertical row of white dots, one determines that the 2D array of white dots correspond to a projection of a 3D array of points deduced from symmetries of $R3c$ space-group applied to $x=\frac{1}{3},y=\frac{2}{3},z=0$ (the yellow balls in Fig. 7(b)).

Table 2
Symmetry of special projections for the space-groups $R3c$, $R\bar{3}c$ and related maximal non-isomorphic subgroups.

	[111]	$[1\bar{1}0]$	$[2\bar{1}\bar{1}]$
$R3c$	$p31m$	$p1$	$p1g1$
$R3$	$p3$	$p1$	$p1$
$R\bar{3}c$	$p6mm$	$p2$	$p2gm$
$R\bar{3}$	$p6$	$p2$	$p2$
$R32$	$p3m1$	$p2$	$p11m$

However, at variance with the result of X-ray diffraction, a full agreement with the $R3c$ space-group is not fulfilled because the periodicity of alternating bands of gray and dark contrast in between these vertical rows of large white dots is not d_{222} but d_{111}.[4] A period equals to d_{111} is confirmed when looking at the lamellae of trigonal structure in between two parts of monoclinic structure, shown in (c). There is an inversion of contrast between (b) and (c) due to different conditions of focalization of the objective lens.

Besides, from the dissymmetric positions of the gray dot rows observed within dark bands in (b), the overall symmetry of the projection is actually $p1$ and therefore characteristic of the space-group $R3$. It results that both opposite directions of the [111] polar axis can be distinguished on this HRTEM image. Thus, polarity inversions, which could be characteristic of a ferroelectric phase, can be identified from small horizontal shifts of gray dots within the dark bands. For instance, as it can be observed on the left part of image (a) the gray dots which appear progressively shifted from the left to the right along the $[\bar{1}01]$ direction of dark bands could be characteristic of an inversion of polarity along the [111] polar axis.

Considering that the monoclinic 11L-Ta_2O_5 (or 25L) structure is likely piezoelectric [22] with a space-group $P112$, both polar axes $[001]_o$ and $[111]_R$ remain therefore parallel through the phase transformation.

Along a $[\bar{1}01]$ zone axis, dissymmetric contrast variations with respect to a two-fold rotation ($p2$) are observed (Fig. 8(a)). Therefore, the symmetry of the $[\bar{1}01]$ projection is $p1$ in agreement with both space-groups $R3$ and $R3c$. Moreover, this dissymmetric contrast is not inverted through both (111) twin planes. Thus, instead of twin planes, (111) stacking faults have to be considered (since the characteristic of a twin plane is to be a mirror plane). It is verified that the relative positions of the crystal lattices on either side of a stacking fault are actually characterized by a translation vector $\frac{1}{3}(0,\bar{1},1)$ parallel to the stacking fault and which the projection along a $[\bar{1}01]$ zone axis corresponds to $\frac{1}{6}(1,\bar{2},1)$ (inset of Fig. 8(a)).

From the indexing of the SAED pattern related to these (111) stacking faults in Fig. 8(a) both $(\bar{1}\bar{4}\bar{1})$ and (101) planes are parallel between domains on either sides of a (111) stacking fault since the reflection $(\bar{1}\bar{4}\bar{1})$ superimposes to a reflection of the type (303). The HRTEM image (a) shows that a stacking fault lamellae can also be ended by a boundary corresponding to habit planes $(101)\|(\bar{1}\bar{4}\bar{1})$. Along a [111] zone axis, a stacking fault lamellae ended by such a boundary gives rises to a change in the fringe lattice (Fig.8(b)). In the upper part of the image, the fringe lattice and corresponding FFT are related to a domain without stacking fault while both fringe lattice and corresponding FFT in the bottom part are related to a domain with one (or several) (111) stacking faults. The 2D lattice resulting of (111) stacking faults is $\sqrt{3}$ times larger and corresponds to a sum of two projected trigonal lattices related by a 60° rotation around the three-fold axis plus the translation $\frac{1}{3}(0,\bar{1},1)$. Along the [111] projection, the

[4] Note that the *hhh* reflections with *h* odd observed on the corresponding SAED pattern do not constitute an argument as they can also appear by multiple diffraction effects.

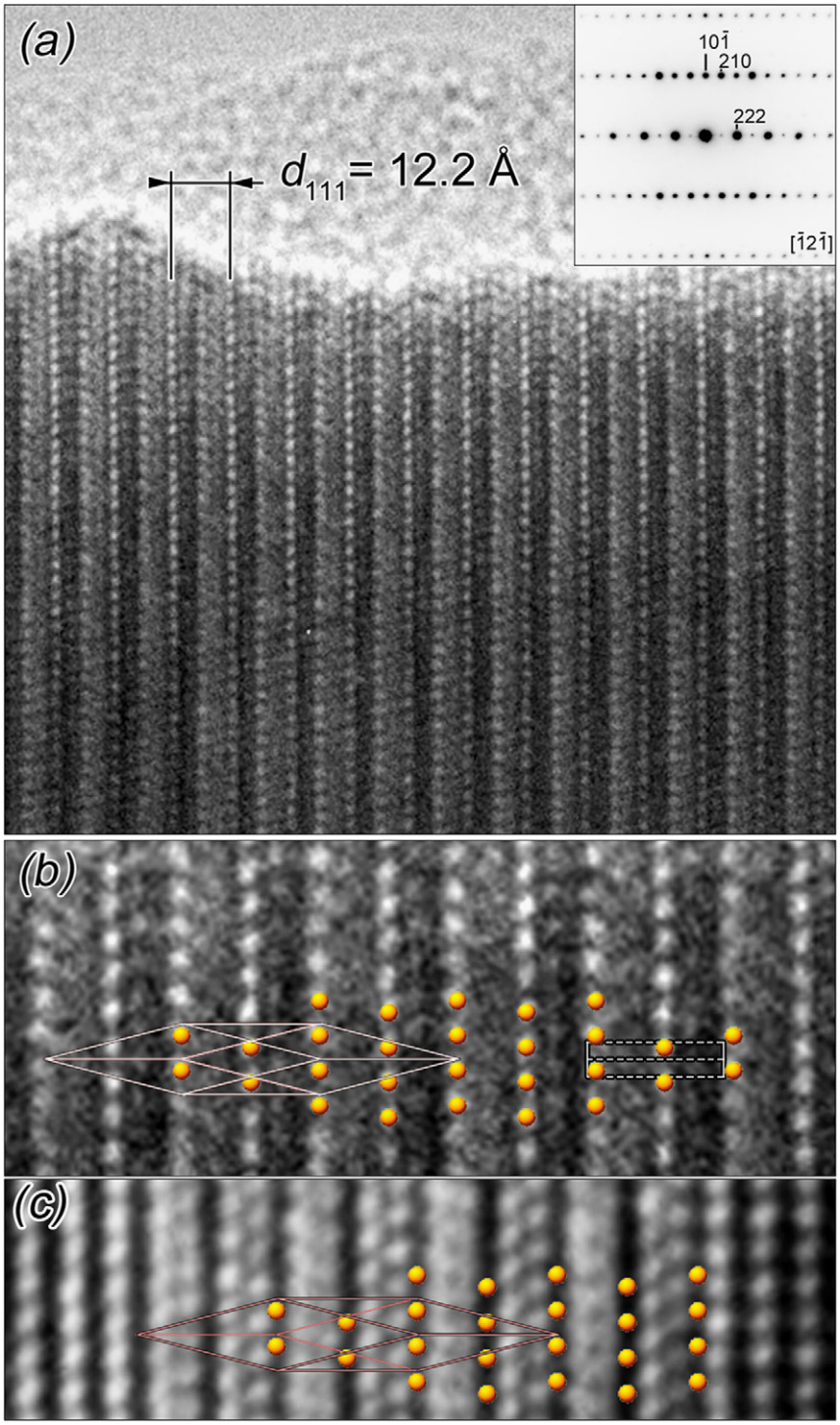

Fig. 7. (a) HRTEM image of the trigonal structure with corresponding SAED pattern of rhombohedral [$\bar{1}$2$\bar{1}$] zone axis and (b, c) analysis of the symmetry *p*1 characteristic of the non-centrosymmetric space-group R3. The image in (c) corresponds to a lamellae of trigonal structure in between two monoclinic parts viewed along a zone axis $[010]_o \| [\bar{1}2\bar{1}]_R$. The objective lens focalization was different between (a,b) and (c). (see text). (For interpretation of the references to color in this figure legend, the reader is referred to the web version of this article.)

stacking fault lamellae appear to be limited along a line of [0$\bar{1}$1] direction in agreement with the result of image analysis of (a). The observed symmetry of a [111] projection of a non-faulted domain being *p*6*mm* for an origin at the center of a hexagon, a non-centrosymmetric space-group *R*3 or *R*3*c* cannot be identified along this projection.

Sufficient information is now available to consider the way Ta atoms could be rearranged in the transformation monoclinic → trigonal. Since the number of Ta atoms are kept, the gathering of two $(001)_o$ Ta–O planes on three (Fig. 6) must correspond to a splitting of Ta atoms in a ratio such that (i) integer number of atoms per 2D hexagonal unit cell (a_{hex} = 6.194(6) Å, $\gamma = 120^\circ$) are obtained after splitting, (ii) atoms can be rearranged in three-fold symmetry within the 2D hexagonal unit cell and (iii) most of the Ta atomic sites must be in agreement with a symmetry space-group *R*3*c*. This 2D hexagonal cell is obtained through a small rearrangement of Ta

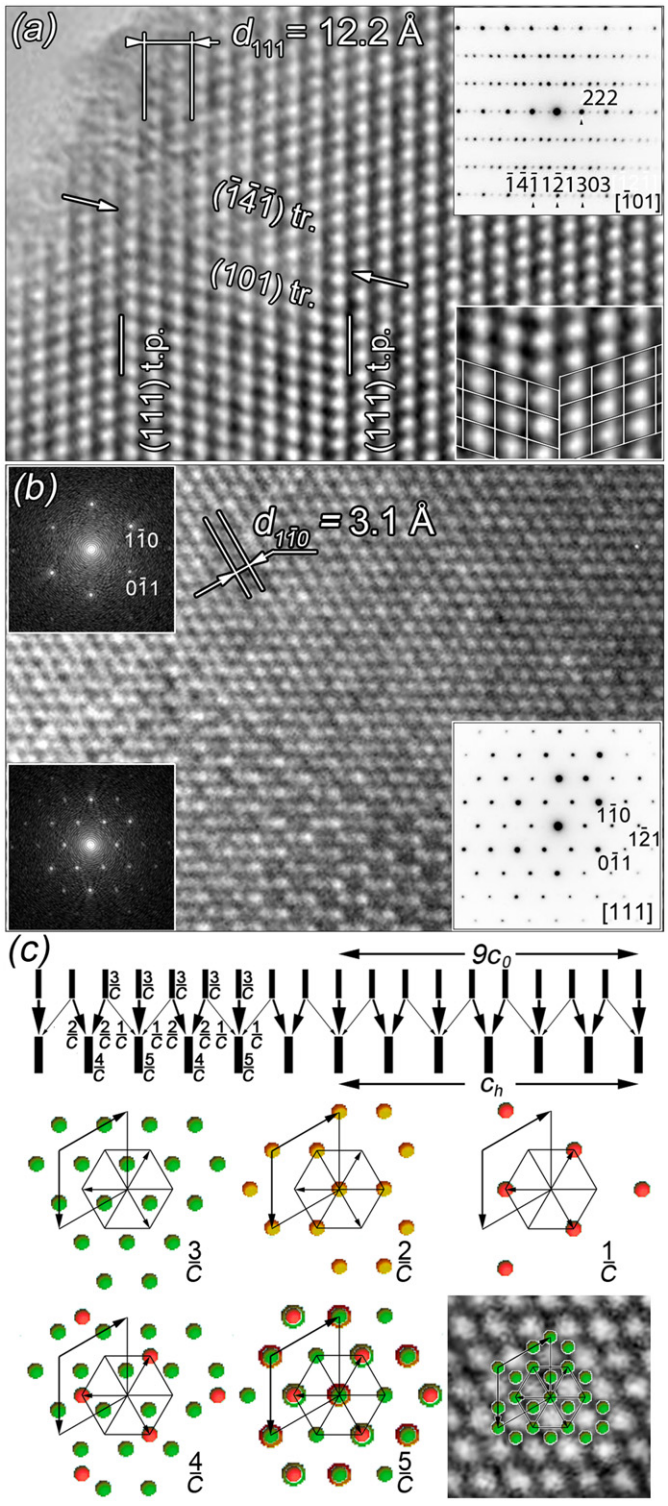

Fig. 8. (a) A (111) stacking fault lamellae terminated by a boundary with habit planes (101)∥($\bar{1}4\bar{1}$); (b) changes in the fringe pattern of [111] zone axis between domains with and without (111) stacking faults; (c) interpretation of the arrangement of Ta atoms in the trigonal structure (see text). (For interpretation of the references to color in this figure legend, the reader is referred to the web version of this article.)

atoms of the (001) plane observed in Fig. 2. It is straightforward to see that the 2D hexagonal cell contains 3 Ta. Therefore, a splitting in fractions of one third and two third can be considered in order to form Ta layers of the trigonal structure. The schema in the upper part of Fig. 8(c) indicates that for identical monoclinic Ta–O planes noted $3/C$, one obtains two types of layer $2/C+2/C=4/C$ and $1C+3/C+1/C=5/C$ in accordance with a d_{111} periodicity. The possibility to rearrange Ta atoms in three-fold symmetry is shown in the following of Fig. 8(c). The Ta atoms of the (000) monoclinic plane, rearranged in an exact six-fold symmetry are represented in green (plane layer $3/C$). This layer can be separated into two layers of trigonal symmetry: $2/C$ in yellow and $1/C$ in red. Then two corrugated layers $4/C$ and $5/C$ can respectively be obtained from a rearrangement of $2/C+2/C$ into $3/C+1/C$ and a superimposition of $1/C+3/C+1/C$. Finally a good agreement is obtained by superimposing layers $4/C$ and $5/C$ on a high resolution image.

In the 3D space, atomic coordinates of Ta (and O) sites, expressed in the *R*3 space-group (rhombohedral axes) must satisfy a null structure factor (or nearly) for the *hhl* reflections with $l=2n+1$ in order to obtain an agreement with the X-ray diffraction results. However, it must also be verified that coordinates of all atomic sites can be expressed only in the *R*3 space-group. Atomic site coordinates for both layers $3/C$ at $(2n+1)\mathbf{c}_{hex}/6$ and $n\mathbf{c}_{hex}/3$ are straightforward to determine (Ta(1) to Ta(6) in Table 3). Through a translation $\frac{1}{3}(0,\bar{1},1)$ of the origin, these coordinates satisfy to the general Wyckoff positions 6*b* of *R*3*c*, namely $/x,y,z/y,z,x/z,x,x,\ y/y+\frac{1}{2},x+\frac{1}{2},z+\frac{1}{2}/x+\frac{1}{2},z+\frac{1}{2},y+\frac{1}{2}/z+\frac{1}{2}$, $y+\frac{1}{2},x+\frac{1}{2}/$ with $x,y,z=\frac{1}{3},\frac{2}{3},0$. The atomic sites of layers $1/C$ being all along the three-fold axis have coordinates of the type *x*,*x*,*x*. In this case, a translation of the origin of the type $\frac{1}{3}(0,\bar{1},1)$ is forbidden because the three-fold symmetry would not be anymore relevant. Only a translation $\frac{1}{2},\frac{1}{2},\frac{1}{2}$ along the three-fold axis can be assumed in order to obtain the Wyckoff positions 2*a* of *R*3*c*. Thus, adding 2 Ta sites in *x*,*x*,*x* and $x+\frac{1}{2},x+\frac{1}{2},x+\frac{1}{2}$, in between adjacent $3/C$ layers we have verified that the Ta partial structure factor for *hhl* reflections:

$$F(hhl)=f_{Ta}\sum e^{i2\pi\mathbf{Q}(hhl)\mathbf{r}}=f_{Ta}\left[\cos\frac{8\pi h}{6}\left(2\cos\frac{2\pi l}{6}+2\cos\frac{4\pi l}{6}\right)\right.$$
$$+(-1)^l+1+6\cos\frac{\pi(2h+l)}{2}\left(\cos\pi(2h+l)\left(2x-\frac{1}{2}\right)\right.$$
$$\left.\left.+i\sin\pi(2h+l)\left(2x-\frac{1}{2}\right)\right)\right]$$

is equal to zero for $l=2n+1$.

As 3 Ta atoms have to be positioned, a solution for keeping a structure factor equal to zero is to assume 2 times 2 sites /*x*,*x*,*x*/

Table 3
Coordinates of Ta atomic sites in *R*3 space-group, which exhibit reflection conditions similar to those of *R*3*c*.

Ta sites	*x*	*y*	*z*	Occ.	Layer
Ta(1)	$\frac{1}{2}$	$\frac{5}{6}$	$\frac{1}{6}$	1	$\frac{3}{C}$ at $(2n+1)\mathbf{c}_{hex}/6$
Ta(2)	$\frac{5}{6}$	$\frac{1}{6}$	$\frac{1}{2}$	1	$\frac{3}{C}$ at $(2n+1)\mathbf{c}_{hex}/6$
Ta(3)	$\frac{1}{6}$	$\frac{1}{2}$	$\frac{5}{6}$	1	$\frac{3}{C}$ at $(2n+1)\mathbf{c}_{hex}/6$
Ta(4)	0	0	0	1	$\frac{3}{C}$ at $n\mathbf{c}_{hex}/3$
Ta(5)	$\frac{1}{3}$	$\frac{1}{3}$	$\frac{1}{3}$	1	$\frac{3}{C}$ at $n\mathbf{c}_{hex}/3$
Ta(6)	$\frac{2}{3}$	$\frac{2}{3}$	$\frac{2}{3}$	1	$\frac{3}{C}$ at $n\mathbf{c}_{hex}/3$
Ta(7)	x_1	x_1	x_1	0.75	$\frac{1}{C}$
Ta(8)	$\frac{1}{2}+x_1$	$\frac{1}{2}+x_1$	$\frac{1}{2}+x_1$	0.75	$\frac{1}{C}$
Ta(9)	$-x_1$	$-x_1$	$-x_1$	0.75	$\frac{1}{C}$
Ta(10)	$\frac{1}{2}-x_1$	$\frac{1}{2}-x_1$	$\frac{1}{2}-x_1$	0.75	$\frac{1}{C}$

$x+\frac{1}{2},x+\frac{1}{2},x+\frac{1}{2}$/ with an occupation factor of 0.75 (Ta(7) to Ta(10) in Table 3). We assume a unique value x_1 for all these sites but two different values x_1, x_2 yields also a structure factor equal to zero.

The Ta–Ta interatomic distance between first neighbors in layers $3/C$ is $a_{hex}/\sqrt{3}=3.58$ Å. A value of $x_1=\frac{1}{12}$ can be chosen such that each of the atomic sites Ta(7), Ta(8), Ta(9) and Ta(10) are surrounded by 1 Ta at 3.05 Å and 3 Ta at 3.68 Å. Increasing or decreasing the x_1 value introduce Ta–Ta distances shorter than 3.05 Å.

It is interesting to note that such short Ta–Ta distances found by Arakcheeva et al. [30] in hexagonal tantalum bronzes with variable compositions are attributed to distances between Ta^{5+} and partly reduced tantalum cations. Thus, assuming that Ta atoms in red and yellow in Fig. 8(c) correspond to Ta^{4+}, the rhombohedral cell might contain 6 Ta^{5+} and 3 Ta^{4+}. Then, balancing of electrical charge implies for instance 6 groups of 3 equivalent O^{2-} sites in between Ta layers (giving rise to TaO_6 octahedra and/or TaO_4 tetrahedra) and 2 groups of 2 equivalent O^{2-} sites with an occupation factor of 0.75, along the three-fold axis. The structure factor incorporating these groups should remain equal to zero for *hhl* reflections with $l=2n+1$. The trigonal phase would have in this case a stoichiometry Ta_3O_7 and the monoclinic-to-trigonal phase transformation will occur via oxygen diffusion. It could also be a good reason explaining that a similar phase transformation was not observed in bulk Ta_2O_5 samples for which several thermal treatments at about 1000 °C under air with varying cooling rate from rapid cooling to a slow cooling at 0.1 ° C min^{-1} have been tried [15]. In this case, a phase transformation was nevertheless observed but it was a second order incommensurate phase transformation occurring very slowly on cooling from 1000 °C. XPS analyses were therefore conducted in order to examine the potential presence of Ta^{4+} cations.

Parallel angle resolved XPS (PARXPS) measurements were performed on a customized Theta 300 spectrometer from ThermoFisher Scienti \ THORNc, using an Al monochromatic source.

Fig. 9(a,b) shows O 1*s* and Ta 4*f* XPS spectra with their curve fitting lines for tantalum oxide thin films of monoclinic (a) and trigonal (b) structures. The peak positions are very similar for both structures. O 1*s* is at 531.1 eV for the monoclinic and 531 eV for the trigonal; the Ta doublet $4f_{7/2}-4f_{5/2}$ is at 26.4–28.3 eV for the monoclinic and 26.3–28.2 eV for the trigonal. According to Atanassova [31] who performed detailed XPS analyses on thin RF sputtered and thermal Ta_2O_5 on Si for high density DRAM application, such binding energies are typical of Ta and O chemical states in Ta_2O_5. The presence of sub-oxides of tantalum, as observed by Atanassova for very thin films a few nanometers thick, should give rise to a peak broadening of Ta 4*f* to a lower binding energy.

Therefore, on account of 22.5 O atoms for 9 Ta atoms, oxygen sites could correspond to 3 groups of 3+3 oxygen sites, which through a translation $\frac{1}{3}(0,\bar{1},1)$ of the origin, are equivalent to the general Wyckoff positions 6*b* of *R*3*c* and 3 groups of 2 oxygen sites with an occupation factor of 0.75, equivalent to the Wyckoff positions 2*a* of *R*3*c*. If, as previously suggested, there are 1 group of 3+3 Ta and 2 groups of 2 tantalum sites with an occupation factor of 0.75, we can assume that these 2 Ta sites are also partly occupied by oxygen atoms, with an occupation factor of 0.25. Therefore, the net volume expansion through the monoclinic-to-trigonal transition would correspond to an introduction of 0.5 oxygen vacancy. As the cell volume is mainly due to the assembly of O^{2-} of large ionic radius (1.35 Å) compared to this of Ta^{5+} (0.64 to 0.74 Å, depending on the coordinance), the value of volume expansion of 1.0207 presently determined, is actually close of a ratio of oxygen sites 23/22.5=1.0222.

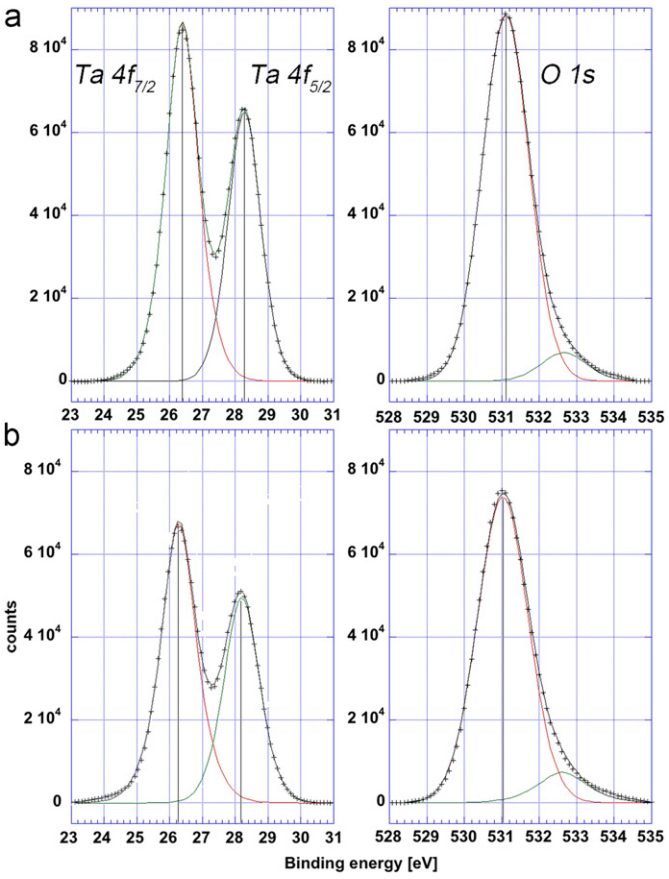

Fig. 9. Comparison between XPS spectra of tantalum oxide thin films of (a) monoclinic and (b) trigonal structures. The background has been subtracted.

As last remark on this TEM study, we have found that the structure of tiny fragments without (111) stacking faults is systematically triclinic instead of trigonal. For instance, angular departures up to about 1.3° from 90° were observed between 111 and $11\bar{2}$ lattice fringes. Since the structure was always trigonal for fragments exhibiting a number of stacking faults, it seems that a stress relaxation, possibly combined with an electric polarization, occurs in this case.

4. Discussion and conclusion

The present results showed that a new trigonal structure of Ta_2O_5 presents probably an interesting piezoelectric property. Several crystallographic aspects of this phase appeared to be in favor of such a property. A high density of electrical dipoles of high momentum along the three-fold axis is likely related to the elongated prolate rhombohedral cell shape. For instance, with respect to piezoelectric perovskite compounds, the number of dipole moments per unit volume could be double. High magnitudes of dipolar momentum could be related to the large expansion coefficient of 4.5% along the three-fold axis observed through the monoclinic-to-trigonal transition, which exhibit the unusual property to occur with increasing symmetry on cooling. The non-centrosymmetry of the trigonal phase appears to be very pronounced. However, if a space-group, either *R*3*c* or $R\bar{3}c$ is inferred to results of X-ray and electron diffraction, the symmetry observed on a special projection $[2\ \bar{1}\ \bar{1}]$ by HRTEM is curiously reduced to *R*3. We have verified that depending on particular atomic site positions in *R*3, the structure factor can imply reflection conditions corresponding to those of *R*3*c*. Nevertheless,

observing a periodicity d_{111} instead of d_{222} on HRTEM images seems to be induced by the electron beam. In this case, an electrical field can be considered through a very thin sample as the result of an electron beam energy loss by excitation of volume plasmons. The electron beam entering the sample represents a current density which polarize the medium, so that the electric field resulting from this polarization interacts with the incoming electron. It acts against the electron, so that it loses an energy per path length unit [32].

It has been outlined that instead of a reversible monoclinic–trigonal Ta_2O_5 phase transition, a bulk Ta_2O_5 material exhibit a second order phase transformation through a very slow cooling from 1000 °C [15]. It seems therefore that reasons for such a change would be due to a difference in surface/volume energy ratios between thin film and bulk materials and perhaps to the energy of interface between Ta_2O_5 and the SiO_2 layer of Si substrates.

Preliminary results on birefringent and piezoelectric properties are presented in part II [33].

Acknowledgments

We thank Bernard Pélissier and Laurent Dussault (Laboratoire des technologies de la microélectronique, CEA-LETI, Grenoble) for the XPS analyses.

References

[1] N. Terao, Jpn. J. Appl. Phys. 6 (1967) 21–34.
[2] R.S. Roth, J.L. Waring, H.S. Parker, J. Solid State Chem. 2 (1970) 445–461.
[3] R.S. Roth, N.C. Stephenson, in: L. Eyring, M. O'Keeffe (Eds.), The Chemistry of Extended Defects in Non-Metallic Solids, North-Holland, Amsterdam, 1970, pp. 167–181.
[4] N.C. Stephenson, R.S. Roth, Acta Crystallogr. B 27 (1971) 1010–1017.
[5] N.C. Stephenson, R.S. Roth, Acta Crystallogr. B 27 (1971) 1018–1024.
[6] N.C. Stephenson, R.S. Roth, Acta Crystallogr. B 27 (1971) 1031–1036.
[7] N.C. Stephenson, R.S. Roth, Acta Crystallogr. B 27 (1971) 1037–1044.
[8] I.E. Grey, W.G. Mumme, R.S. Roth, J. Solid State Chem. 178 (2005) 3308–3314.
[9] S. Schmid, K. Fütterer, J.G. Thompson, Acta Crystallogr. B 52 (1996) 223–231.
[10] S. Schmid, R.L. Withers, J.G. Thompson, J. Solid State Chem. 99 (1992) 226–242.
[11] A.D. Rae, S. Schmid, J.G. Thompson, R.L. Withers, N. Ishizawa, Acta Crystallogr. B 51 (1995) 709–721.
[12] S. Schmid, J.G. Thompson, A.D. Rae, B.D. Butler, R.L. Withers, N. Ishizawa, S. Kishimoto, Acta Crystallogr. B 51 (1995) 698–708.
[13] S. Lagergren, A. Magneli, Acta Chem. Scand. 6 (1952) 444–446.
[14] K. Lehovec, J. Less-Common Metals 7 (1964) 397–410.
[15] M. Audier, B. Chenevier, H. Roussel, A. Lintanf Salaün, J. Solid State Chem. 183 (2010) 2068.
[16] Y. Nakagawa, Y. Gomi, Appl. Phys. Lett. 46 (1985) 139–140.
[17] Y. Nakagawa, Y. Gomi, T. Okada, J. Appl. Phys. 61 (1987) 5012–5017.
[18] Y. Nakagawa, T. Okada, J. Appl. Phys. 68 (1990) 556–559.
[19] S. Kakio, T. Mitsui, A. Tsuchiya, Y. Nakagawa, 2009 IEEE International Ultrasonics Symposium Proceedings, 2009, p. 2643.
[20] B.R. Jooste, H.J. Viljoen, J. Mater. Res. 13 (1998) 475–482.
[21] H.J. Viljoen, B.R. Jooste, Piezoelectric Sensors/Actuators for Use in Refractory Environments, Patent Number 6,057,628, Date of Patent May 2, 2000.
[22] R. Parmentier, F. Lemarchand, M. Cathelinaud, M. Lequime, C. Amra, S. Labat, S. Bozzo, F. Bocquet, A. Charai, O. Thomas, C. Dominici, Appl. Opt. 41 (2002) 3270–3279.
[23] International Centre for Diffraction Data, JCPDS Card No. 25-0922, ICDD, Newton Square, PA, 1996.
[24] A. Lintanf-Salaun, A. Mantoux, E. Blanquet, E. Djurado, J. Electrochem. Soc. 156 (2009) H311–H315.
[25] A. Lintanf-Salaun, Dépots Par ESD et ALD et Caractérisations Physicochimiques de Couches d'Oxydes á l'Échelle Nanométrique Pour la Microélectronique, Thesis, INP-Grenoble, 2008.
[26] Q. Fang, J.-Y. Zhang, Z.M. Wang, J.X. Wu, B.J. O'Sullivan, P.K. Hurley, T.L. Leedham, H. Davies, M. Audier, C. Jimenez, J.-P. Senateur, I.W. Boyd, Thin Solid Films 428 (2003) 242–248.
[27] P. Stadelmann, Java Electron Microscope Simulation Software, ⟨http://cimewww.epfl.ch⟩.
[28] J. Schenck, J. Primot, R. Von der Muhll, J. Ravez, Solid State Commun. 21 (1997) 57–60.
[29] International Tables for Crystallography, vol. A, Th. Hahn (Ed.), Reidel, Dordrecht, 1983.
[30] A.V. Arakcheeva, G. Chapuis, V.V. Grinevich, V.F. Shamrai, Crystallogr. Rep. 49 (2004) 70.
[31] E. Atanassova, Microel. Reliab. 39 (1999) 1185.
[32] H. Raether, Excitation of Plasmons and Interband Transitions by Electrons, Springer Tracts in Modern Physics, vol. 88, Springer, Berlin, Heidelberg, 1980, pp. 23–34.
[33] M. Audier, B. Chenevier, H. Roussel, L. Vincent, A. Peña, A. Lintanf Salaün, J. Solid State Chem., Part II, in this issue, doi:10.1016/j.jssc.2011.06.002.